Advances in Geo-Energy Research

Vol. 9, No. 3, p. 198-210, 2023

Original article

# Response law and indicator selection of seismic wave velocity for coal seam outburst risk

Liming Qiu[1,2], Yi Zhu[1], Qiang Liu[1], Minggong Guo[2], Dazhao Song[1]*, Anhu Wang[3]

[1]*State Key Laboratory of the Ministry of Education of China for High-efficient Mining and Safety of Metal Mines, University of Science and Technology Beijing, Beijing 100083, P. R. China*

[2]*Pingdingshan Tianan Coal Mining Co., Ltd., Pingdingshan 467099, P. R. China*

[3]*Technical Support Centre for Prevention and Control of Disastrous Accidents in Metal Smelting, University of Science and Technology Beijing, Beijing 100083, P. R. China*

**Keywords:**
Seismic wave computed tomograph
coal seam stress field
wave velocity anomaly coefficient
wave velocity gradient

**Cited as:**
Qiu, L., Zhu, Y., Liu, Q., Guo, M., Song, D., Wang, A. Response law and indicator selection of seismic wave velocity for coal seam outburst risk. Advances in Geo-Energy Research, 2023, 9(3): 198-210.
https://doi.org/10.46690/ager.2023.09.07

**Abstract:**
The accurate detection of coal seam stress field effectively prevents coal and gas outbursts. This study uses wave velocity, wave velocity anomaly coefficient, and wave velocity gradient as indicators to identify stress anomalies in coal seam. The results show that these three indicators of wave velocity are all positively correlated with load, while changes in the wave velocity anomaly coefficient and wave velocity gradient are more gentle than those of wave velocity. The degree of damage of coal can be judged by the wave velocity anomaly coefficient, while the transition between high and low stress zones can be identified by the wave velocity gradient. In areas affected by geological structures such as valleys and mountain tops, the coal seam wave velocity and wave velocity anomaly coefficient may exhibit anomalies. The comparative analysis of wave velocity and its derived indicators can reveal the stress state and coal structure of coal seamwith higher accuracy, identify the areas affected by geological structures such as valleys and mountain tops, and determine the boundary of the stress relief zone after hydraulic fracturing. Combined with the actual geological structure characteristics of coal seam, it can accurately identify the stress disturbance region of coal seam and achieve the purpose of predicting coal and gas outbursts.

## 1. Introduction

As one of the five kinds of natural disaster in coal mines, coal and gas outburst invariably endangers safe production. With the increasing depth and intensity of coal mining, the risk of coal seam outburst also gradually increases (Aguado and Nicieza, 2007; Vlastimil and Milan, 2010; Zhao et al., 2023). Therefore, the prediction of outburst disaster risk has become increasingly important, and the means to accurately predict outburst disasters have been widely concerned by scholars in this field (Koziel and Janus, 2022; Mlynarczuk and Skiba, 2022; Li et al., 2023). After a long period of exploration, many researchers at home and abroad have conducted relevant studies on outburst prediction (Qiu et al., 2020; Fatemeh et al., 2023). From previous similarity experiments, to the analogy of coal structure, observation of outburst events, to contact detection in advance of drilling in the working area, outburst prediction technology has summarized some risk prediction methods (Qiu et al., 2019; Xu and Fu, 2021). These mainly include: single index method, prominent prediction comprehensive index method, comprehensive geological index method, gas geological region prediction and gas geological unit method, etc. The risk prediction of excavation face is to determine the outburst risk of coal body, that is, local prediction. The existing working face prediction methods are mainly drilling cuttings, gas desorption method, drilling gas initial velocity method, and so on (Khadijeh et al., 2021; Zhang et al., 2022). The above methods mostly use sampling and fixed-point indicators, the drilling works are large, and the

*Corresponding author.
*E-mail address*: qiulm@ustb.edu.cn (L. Qiu); zhuyi980315@163.com (Y. Zhu); liuqiang_2215@163.com (Q. Liu); pingmeigmg@126.com (M. Guo); song.dz@163.com (D. Song); anhu163@163.com (A. Wang).

Received August 10, 2023; revised August 28, 2023; accepted September 15, 2023; available online September 18, 2023.

Yandy Scientific Press

human factors cause great interference and usually affect the production to a certain extent (Xue et al., 2022). In the time domain, continuous monitoring cannot be achieved, while in the space domain, it is reflected in the form of "point evaluation", which is difficult to reflect the regional coal rock stress environment and the dynamic evolution process of coal and gas outburst risk during the mining disturbance process (Shi et al., 2020). Importantly, these traditional methods can neither achieve the purpose of visual monitoring of the drilling process nor be dynamically adjusted in time due to the limitations of drilling methods. Besides, the accuracy of monitoring methods still needs to be improved.

The above prediction methods mainly focus on local prediction, that is, mostly the prediction indicator of gas concentration, while the research on coal seam stress has been less sufficient. In geological history, the formation process of coal and gas is very complex (Liu et al., 2022), and the risk of coal and gas outburst is not only affected by gas pressure and content. Regarding coal and gas outburst, scholars have not only studied the mechanism (Zykov and Lee, 2016; Zheng et al., 2023) but also explored the prediction means and prevention technology (Frid and Vozoff, 2005; Hudecek, 2008; Jun et al., 2016; Yang et al., 2021). These outbursts primarily occur in high gas coal mines and mines with outburst risk tendency (Black, 2019). Despite that there have been many low-gas level outburst accidents at home and abroad, the problems of coal and gas outburst in low-gas coal mines have not been paid sufficient attention to by society or thoroughly explored by academics. The first reported low-gas outburst accident occurred in Poland, and the lowest gas pressure at the time of outburst was only 0.3 MPa (Lamaet and Bodziony, 1998). Bai et al. (2009) calculated the abnormal gas dynamic phenomenon of Xinmi coal field, which is mainly mined by Zheng Coal Group. The outburst gas pressure of Peigou mine in this area is only 0.5 MPa, which is far lower than the critical value of gas pressure stipulated by China's coal industry code. Regarding the phenomenon of coal and gas outburst in low-gas mines, scholars have put forward the hypothesis that the outburst practice of low-gas mines occurs under the condition of low gas in the outburst source area, and that gas may not be the main driving force for the outburst (Yan et al., 2015). Instead, the abnormal stress field or other geological conditions are likely to play a leading role, which is different from rock burst in the general sense; a deep complex geological structure or ground stress field may be behind this phenomenon (Katarzyna et al., 2022). The key to uncover the mechanism is to study the physical and mechanical properties of abnormal coal and rock mass and the local complex ground stress state. To this end, the distribution characteristics of the geo-stress field in a certain spatial range of the boundary of the outburst source region can be studied (Alexander and Yuliya, 2019). At the same time, it is necessary to conduct stress detection in areas with low gas level. Currently, there is a lack of methods for stress field detection, and relevant research mainly includes stress meters and in-situ testing methods (Sobczyk, 2014). However, all of these methods monitor stress at points or in a small range and adopt the "point with surface" method to achieve the purpose of in-situ stress monitoring, which cannot accurately reflect the regional stress field in the well.

As a new geophysical method, seismic wave computed tomograph (CT) technology has been gradually applied to mine engineering and geological diagnosis (Salimbeni et al., 2018; Rezaei et al., 2019; Peng et al., 2023). By analyzing the elastic wave rays between the seismic platform and the mine seismic station, this technology can invert the wave velocity of the exploration area and subsequently evaluate the distribution of the regional stress field, so as to realize the advanced stress detection of the working face and the purpose of accurately reflecting the regional stress field of the mine (Lurka, 2008). Liu et al. (2017) used seismic monitoring technology to observe the activity of hidden faults and predict dynamic disasters. Shu et al. (2022) employed the same technology to monitor the activity of coal seam, recorded seismic signals under different operations, and proposed an effective signal recognition method based on the time-frequency characteristics.

Seismic wave CT technology essentially utilizes seismic monitoring technology to collect seismic signals generated during the process of coal and rock fracture (Li et al., 2007; Durucan et al., 2019). It takes these signals to invert the distribution law of wave velocity in coal and rock masses (Saito et al., 2015; Uyanik, 2019). In the past, this technology was widely used in rock burst mines, and in recent years, it was implemented for detecting stress field in the area of outburst coal seams, which has obvious effects on the prevention and control of coal and gas outburst (Peng et al., 2023). At present, the application of seismic wave CT technology in outburst coal seams mainly focuses on the inversion of longitudinal wave velocity, and the risk of coal and rock dynamic disasters is evaluated based on the positive correlation between wave velocity and the bearing capacity of coal and rock masses. However, there is insufficient research on wave velocity indicators that characterize the outburst risk, and further studies are needed on the relationship between the derived indicators of wave velocity and regional stress fields.

To address the above issues, this study analyzes the correlation between derived indicators of seismic wave velocity and load in coal and rock masses based on laboratory research results to reveal the distribution characteristics of different derived indicators of wave velocity in coal seams. Subsequently, on-site testing and verification is conducted, laying the foundation for predicting outstanding hazards. The findings are helpful for further developing outburst prediction methods and improving the effectiveness of coal and gas outburst prevention and control.

## 2. Experimental method

### 2.1 Experimental system and scheme

In order to test the variation in wave velocity during the loading and failure process of coal, we established an experimental system as shown in Fig. 1. This includes a pressure testing machine, a pressure control computer, two wave velocity testing sensors, two signal amplifiers, a signal acquisition instrument, and a wave velocity data analysis

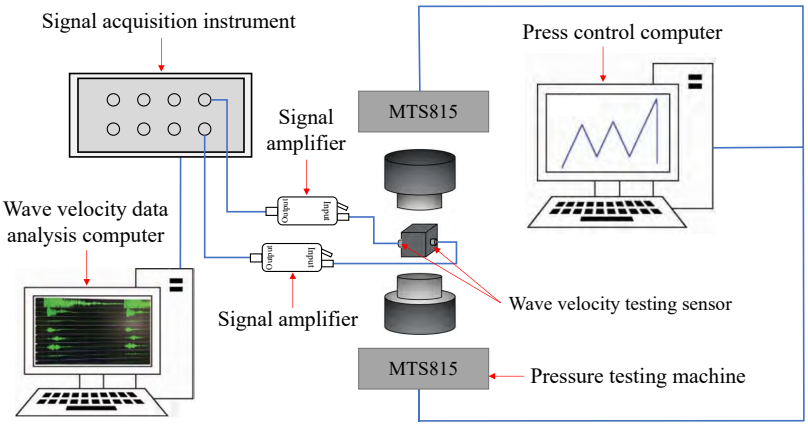


**Fig. 1**. Experimental system for measuring wave velocity during coal loading.

computer.

The MTS815 electro-hydraulic servo rock mechanics tester was adopted as the pressure testing machine in this experiment. MTS815 is a hydraulic servo mechanical system that applies confining pressure to the sample through liquid oil and axial pressure to the upper and lower shaft presses. It has a pneumatic feeding system, which can test various mechanical and seepage characteristics of various coal and rock materials under complex load conditions and complete the loading experiment of coal and rock containing gas.

In the experimental setup, the two wave velocity sensors are attached to the coal sample in a horizontal direction relative to each other. The sensor on the left generates waveform signals, while the sensor on the right receives the signals. The two signal amplifiers with the same amplification ratio are connected to the wave velocity sensors. Once the seismic waveform has been collected, the wave is marked, the excitation point and the initial arrival point of the wave are found, and the time required for the wave to pass through the coal sample is obtained.

The raw coal samples used in the experiment were taken from the No. 22 coal seam of Jinjia coal mine, Guizhou Panjiang Fine Coal Co., Ltd., a typical outburst mine in the Panjiang Mining area. Due to the soft coal quality of Jinjia coal mine outburst coal seam, obtaining a complete raw coal sample through drilling is impossible. Therefore, all the coal samples were cube samples, which were compressed into 100 mm × 100 mm × 100 mm size by pulverized coal, with the end face deviating by no more than 0.05 mm from parallel. The briquette sample processing strictly followed the requirements of measuring the physical and mechanical properties of coal and rock.

After the coal sample was installed, the confining and axial pressure were simultaneously set to 2 MPa. This setting is in compliance with conventional experimental requirements, as the uniaxial compressive strength of the briquette sample is much lower than the triaxial compressive strength of the raw coal. Then, the confining pressure was kept unchanged and the axial pressure was increased until the damage of the sample. To ensure the safety of the experiment, displacement loading

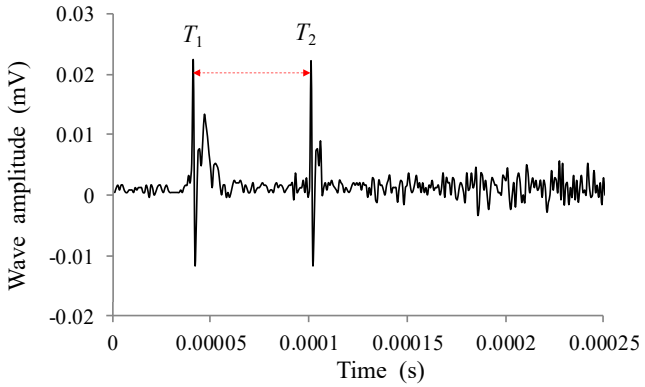


**Fig. 2**. Schematic diagram of longitudinal wave velocity measurement of coal sample.

was selected for all loading sessions in this experiment, and the loading rate was 0.4 mm/min until the damage of coal sample to determine the maximum load at this point.

## 2.2 Calculation method of wave velocity derived indicators

### 2.2.1 Wave velocity indicator

Coal and rock stress field detection is mainly based on the apparent power function relationship between the longitudinal wave velocity of coal and rock wave and the stress magnitude. The greater the stress of coal and rock mass, the greater the propagation velocity of the longitudinal wave. Therefore, the distribution characteristics of stress field in the wave velocity detection region can be realized by inverting the distribution characteristics of longitudinal wave propagation velocity in the coal rock mass.

The seismic wave starting point of the sample is determined according to the method shown in Fig. 2 (Gong, 2010). In the figure, $T_1$ represents the time when the seismic wave begins to propagate, and $T_2$ represents the time for the receiving probe to receive the seismic wave. When the meaning of $T_2 \sim T_1$, it means that the specimen travels through the length $L(1-\varepsilon)$ during loading, where is the axial strain. The time difference

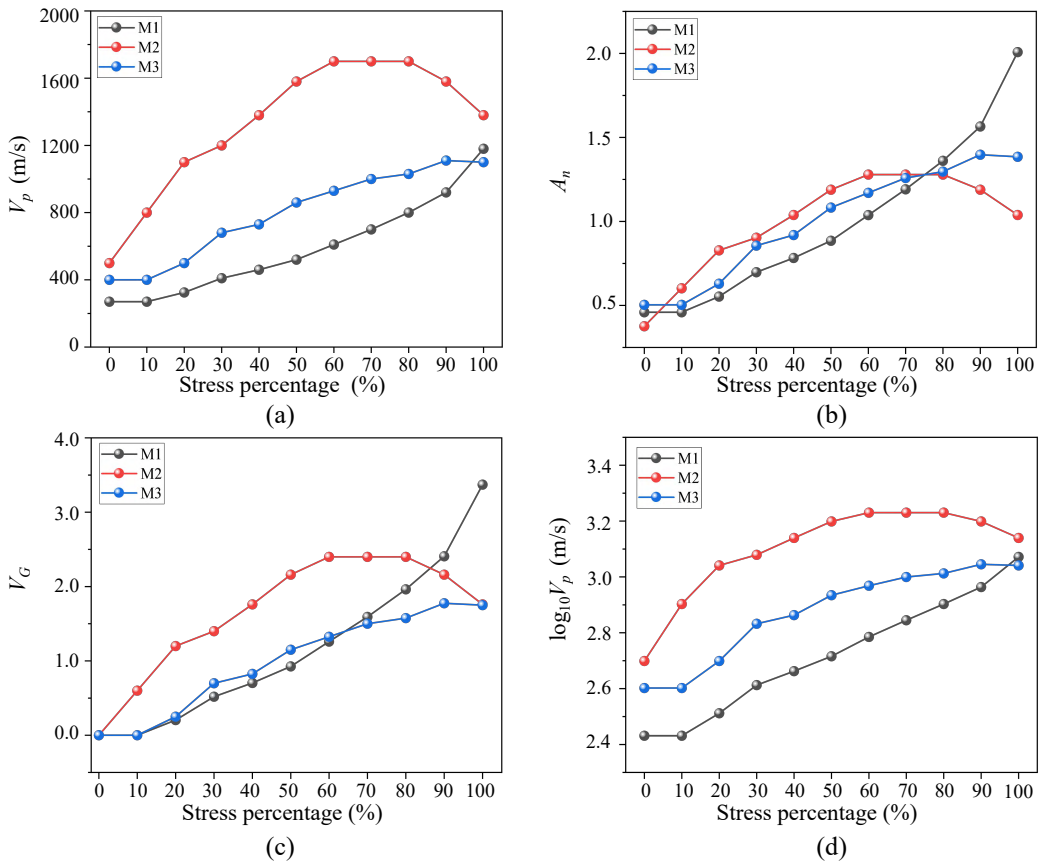


**Fig. 3**. Variation in the wave velocity parameters during coal sample loading: (a) Wave velocity $V_p$, (b) wave velocity anomaly coefficient $A_n$, (c) wave velocity gradient $V_G$, (d) logarithm of wave velocity $\log 10V_p$.

between the time when the pulse voltage of the excitation probe is excited and the time when the receiving probe receives the seismic wave is equal to the time needed for the seismic wave to propagate through the sample, which is indicated by the time difference between the two dashed lines in Fig. 2.

For the waveform signal recorded in the loading process of coal and rock samples, the longitudinal wave velocity can be calculated by:

$$V_p = \frac{L(1-\varepsilon)}{T_2 - T_1} \tag{1}$$

where $V_p$ denotes the seismic wave velocity, $\varepsilon$ denotes the strain and $L$ denotes the height of the sample before loading.

### 2.2.2 Wave velocity anomaly coefficient indicator

The wave velocity anomaly coefficient can be calculated by:

$$A_n = \frac{V_p - V_p^a}{V_p^a} \tag{2}$$

where $A_n$ denotes wave velocity anomaly coefficient, $V_p^a$ denotes the average of the model wave velocity.

In the process of roadway excavation, there will be many cracks and weakening zones in the tectonic zone, and the seismic wave velocity will decrease when passing through them. The degree of rock mass weakening and fracture is related to the magnitude of seismic wave velocity reduction. Therefore, the degree of breakage in the inversion region can be judged by the positive and negative anomalies of seismic wave velocity.

### 2.2.3 Wave velocity gradient indicator

For the wave velocity change recorded in the loading process of coal and rock samples, the gradient of wave velocity is calculated by:

$$V_G = \frac{V_p - V_0}{V_0} \tag{3}$$

where $V_G$ denotes the wave velocity gradient, $V_0$ is the initial wave velocity of the sample without stress.

When there are folds, faults, fracture zones, and other geological structure areas in front of the tunneling roadway, the stress balance in the area will be affected, resulting in uneven stress distribution. According to the experimental relationship between longitudinal wave velocity and load, the fracture zone corresponds to a low wave velocity region, whereas the stress concentration region corresponds to a high wave velocity region. Between these two regions, there is a transition region from high wave velocity to low wave velocity, that is, the region with a large gradient of wave velocity. Existing studies have shown that coal and rock dynamic disasters occur not only in the region of high wave velocity but also in the aforementioned region with obvious wave velocity gradient, which makes it another important outburst risk region.

## 2.3 Experimental results and analysis

The test results of wave velocity and its derived indicators of 3 outburst coal samples during the uniaxial compression experiment are shown in Fig. 3. These three samples are numbered as M1, M2 and M3, respectively.

As shown in Fig. 3(a), the overall trend of the three groups of curves is consistent. The initial wave velocity of sample M1 is 270 m/s, which increases with the stress level and reaches the maximum value when the stress reaches the peak value, which is 1,180 m/s. The value of wave velocity increases by 337% compared to the unstressed state. The initial wave velocity of the M2 sample is 500 m/s, and the maximum wave velocity is 1,700 m/s at 60% of the peak stress. Furthermore, it begins to decline when the stress reaches 80% of the peak stress and finally reaches 1380 m/s, with an overall growth rate of 176%. The initial wave velocity of the M3 sample is 400 m/s and the maximum value is 1,110 m/s, which is located at 90% of the peak stress. The growth rate is 177.8%, similar to that of the M2 sample. The wave velocity of the M2 sample is higher than that of the other two groups in the whole process of loading, and it is still the highest even if it drops later. On the whole, the change trend of curves in the three groups of samples is consistent. This indicates that whether the coal is dense or not, the overall trend of wave velocity change during the loading process is consistent and it increases with the stress level in the early loading stage. That is, the pores in the coal are gradually compressed, but when the compression becomes extremely high, the wave velocity tends to stabilize until the sample is destroyed. Therefore, monitoring the wave velocity change of coal body in the coal seam can accurately reflect the stress concentration in this region.

As shown from Fig. 3(b), the $A_n$ of sample M1 is about 0.4 when not loaded and gradually increases with stress loading. The maximum value is about 2.0 when the stress peaks, higher than the other two groups of samples. For M2 and M3 samples, the $A_n$ of M2 before loading is at the minimum value, that is, less than 0.25, and that of M3 is at the highest value, that is, close to 0.5. After loading, M2 gradually exceeds other samples and drops to the lowest value in the later period. This is because the M2 sample is relatively dense. Although its wave velocity is high in the whole loading process, $A_n$ is basically close to the other two groups of samples in the early stage, and the $A_n$ of M2 sample is even lower than that of M1 and M3 samples at the end of loading. This indicates that in the early loading stage, the $A_n$ value of coal samples with low porosity has the same variation trend as that of samples with high porosity. When microfractures occur during loading, the $A_n$ value begins to decrease.

It can be seen from Fig. 3(c) that the $V_G$ of the three groups of coal samples is small when no load is applied. This is because when the stress starts to rise, the value of M2 sample with low porosity increases rapidly and the growth rate is much higher than that of the other two groups of samples. When the load reaches 60% of the peak stress value, the $V_G$ value of the sample no longer increases but gradually decreases, which is consistent with the change trend of $V_p$ and $A_n$, and has a good corresponding indicator effect. When loaded in the pre-failure stage of the sample, the $V_G$ of sample M1 is at the highest value, which corresponds to the curve of $A_n$ in Fig. 3(b).

It is worth noting that the data of high wave velocity samples can easily conceal the variation pattern of wave velocity in samples with low wave velocity, as seen in Fig. 3(a). To facilitate the analysis, the logarithm of the wave velocity of each sample was taken to obtain three gentle curves, as shown in Fig. 3(d). The general trend in the figure is consistent with the curve in Fig. 3(a), where the wave velocity of each sample shows a more obvious trend of increasing with the stress level and the comparison is more precise. When the stress percentage increases from 10% to 90% of the peak stress, the relation between the wave velocity pair value and the stress percentage is almost linear.

On the whole, for samples with higher overall wave velocity, the $V_G$ and $A_n$ do not necessarily present a high value, while for samples with lower wave velocity, the changes in both parameters are apparent. This indicates that the monitoring of coal sample failure wave velocity should not only focus on the absolute wave velocity. In fact, for coal and rock masses under three-dimensional stress, many of their failure processes stem from unloading or stress gradients, and simply focusing on the absolute value of stress cannot accurately predict the failure of coal and rock masses. Therefore, it is also necessary to pay attention to other derived indicators of wave velocity, such as $A_n$ and $V_G$, for testing the wave velocity field of coal and rock masses. A more accurate and effective inversion of the stress state of coal and rock masses can be obtained by comprehensively considering the laws of multiple indicators of wave velocity parameters, thereby predicting the coal and gas outburst risk.

## 2.4 Analysis of technical application method

Pore fissure in the coal body is an essential factor that causes the change in longitudinal wave velocity. As a porous material, the closing and generation of fissure in coal and rock is closely related to the stress-strain stage under load (Wang et al., 2023; Xu et al., 2023; Ye et al., 2023). The stress-strain curve of the general coal body loading process can be divided into five sections, and the stress-strain characteristics and wave velocity change characteristics at each stage are shown in Fig. 4.

In the initial stage of stress, internal cracks in the coal itself will gradually close under the action of extrusion. At this time, the density of the coal sample keeps increasing, which leads to the increase in the longitudinal wave velocity of the coal body. Then, the coal will enter the elastic stage with continued loading. In this stage, the stress and strain almost form a linear relationship. The wave velocity also presents a linear increase, which has an excellent corresponding relationship. Subsequently, it will go through the transition stage of elasticity and plasticity. Due to the continuous increase in stress, new cracks will form in the coal body, and the seismic wave velocity in this stage will continue to rise. Finally, it goes through the plastic behavior stage. At this time, many new cracks will occur in the rock mass parallel to the loading direction, and the original cracks will also be accelerated until

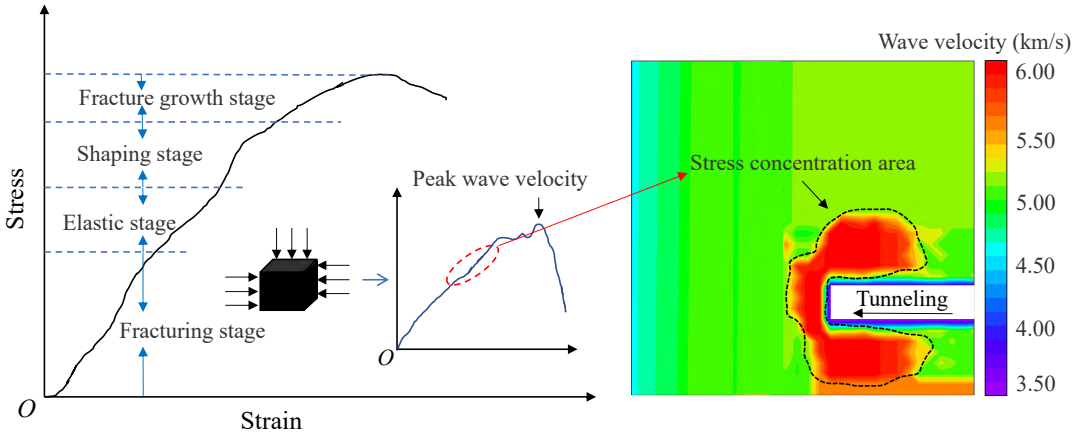


**Fig. 4**. Stress-strain curves and wave velocity curves of coal under load.

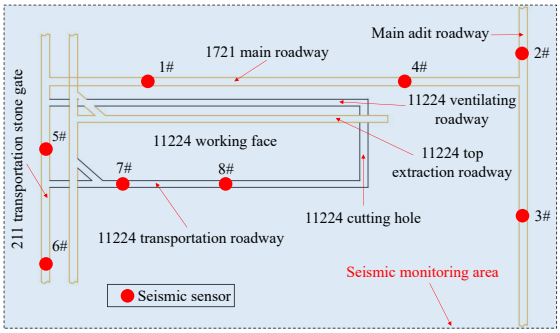


**Fig. 5**. Schematic diagram of wave velocity monitoring during the excavation process in Jinjia coal mine.

damage. Furthermore, the coal sample is faced with the risk of overall failure at any time, and its wave velocity will be violently shaken, that is, its value will fluctuate. When the stress peak is reached, the coal body is destroyed. During this process, various cracks derived from it become gradually larger and many microscopic cracks develop towards macroscopically visible cracks. At this time, the wave velocity of the coal body decreases rapidly until the rock is completely broken. Regarding this stage, there is a good coupling relationship between the stress-strain curve of the coal body under load and the wave velocity change curve.

The distribution of wave velocity $V_p$ in the tunneling roadway area is shown on the right side of Fig. 4. It can be seen that the space of the tunneling roadway corresponds to the lowest wave velocity area. The abnormal area with high wave velocity value is concentrated in front of and around the tunneling roadway, which is more consistent with the stress concentration area caused by the operation disturbance in front of the tunneling roadway. The wave velocity value also gradually decreases and the abnormal wave velocity area on the upper left corresponds to the gas accumulation or high stress area. The inversion results can supplement the coupling relationship between the stress-strain curve and wave velocity curve of coal under load. It is further indicated that the stress concentration degree of coal rock mass in the stress concentration area caused by artificial operations and rock mass structure can be better reflected by wave velocity detection. Based on this and the anomaly indicator of wave velocity presented in Fig. 3, the results of each indicator are combined to confirm each other, thus the location of the abnormal area in the mine can be determined and the purpose of more accurate monitoring can be achieved. In other words, by combining the detection results of seismic wave CT with the working conditions of the site and analyzing the change law of the indicators, we can accurately detect the abnormal area of coal seam stress and further achieve the prediction of coal and gas outburst risk. The indicators used for analysis include wave velocity $V_p$, wave velocity anomaly coefficient $A_n$, and wave velocity gradient $V_G$. Certainly, this can also be $\log_{10} V_P$.

## 3. Verification and application

### 3.1 Verification case 1: Coal seam tunneling

This section takes Jinjia coal mine as the research object. The mine field is located in Panjiang mining area, and the construction location is the 11224 working face, which is situated in the south wing of the shaft 22# coal seam second section. The corresponding area mainly includes the 11224 transportation roadway, the 11224 cutting hole and the 11224 ventilating roadway. The schematic diagram of wave velocity monitoring is shown in Fig. 5.

#### 3.1.1 Distribution of $V_p$ before and after coal seam tunneling

In order to further study the response characteristics of each indicator parameter to the influence of mining technology on the regional stress field of 11224 tunnel in Jinjia coal mine, this section selects the seismic data before and during tunnel excavation for inversion. It obtains the distribution of $V_p$ on the working face of 11224 before and after tunneling in Jinjia coal mine, as shown in Fig. 6.

It can be seen from the figure that before tunneling, the inversion results of wave velocity range from 2.0 to 6.0 km/s, and there are a large number of abnormal areas of wave velocity on the working face. The abnormal area of wave velocity in this area is mainly within the range of 150 m behind the tunneling head of the roadway and 100 m under

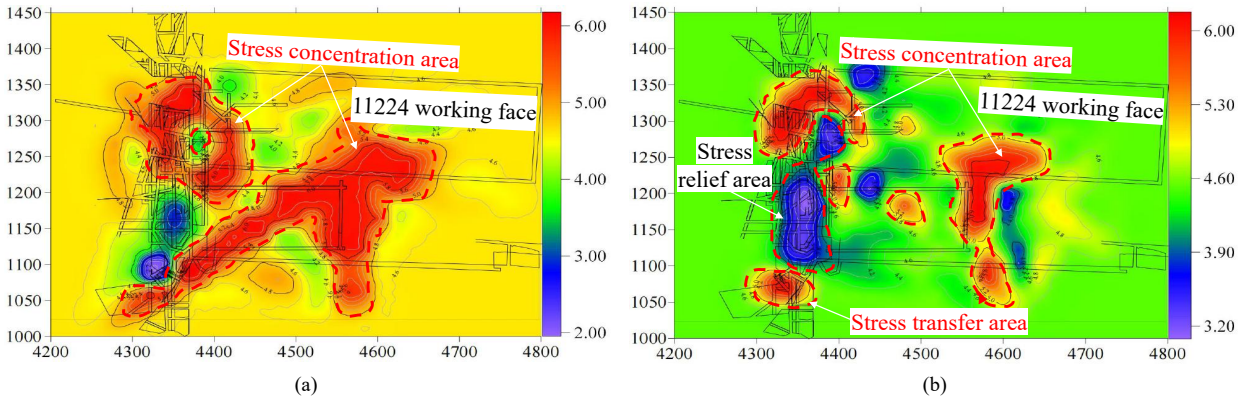


**Fig. 6**. Wave velocity distribution of coal seam before and after tunneling: (a) $V_p$ distribution before tunneling, (b) $V_p$ distribution after tunneling.

the roadway, showing a narrow belt with increased stress and a connected state. The wave velocity is mostly between 4.8 and 6.0 km/s, which is consistent with the position of the surface valley. The cause of this phenomenon may be that there are some gas accumulation areas in the coal seam area before tunneling, which leads to the stress concentration of the surrounding coal and in turn leads to the abnormal wave velocity. During the tunneling period, the overall wave velocity of 11224 working face decreases, which is between 3.2 and 6.0 km/s. The abnormal wave velocity area behind the 11224 transportation roadway decreases compared with the distribution before tunneling, and the wave velocity in some areas drop to below 4.8 km/s. At this time, the abnormal wave velocity area within 30 m in front of the tunneling head indicates a crushing area in the coal stratum, which is mainly due to the subsidence of the roadway roof that causes the upper coal strata to break. The abnormal area of the wave velocity in front of the head is caused by the disturbance of the coal rock stratum in front of the roadway, which is a normal phenomenon. In addition, there is no stress anomaly. The result can confirm the rationality of wave velocity inversion to monitor the stress of outburst coal seam.

### 3.1.2 Distribution of $A_n$ before and after coal seam tunneling

The distributions of wave velocity anomaly coefficient $A_n$ of 11224 on the working face before and after tunneling of 11224 in Jinjia coal mine are shown in Fig. 7. The wave velocity anomaly coefficient $A_n$ in the 11224 working face area before tunneling is between -0.55 and 0.30, and the abnormal area with An greater than 0.1 is relatively large. The reason for this phenomenon may be that there is some gas accumulation in the coal seam area before tunneling, leading to stress concentration in the surrounding coal and then abnormal wave velocity. At the same time, gas extraction carried out before the excavation will also impact this area. After entering the mining period, once the gas extraction in the coal seam has been completed, the affected areas in the coal seam become reduced. The wave velocity anomaly coefficient in the region mostly reduces to a value below 0.05, and the negative anomaly coefficient also increases from −0.55 to −0.30, which is within the safe range. These test results can be used to verify the extraction effect. During this period, it can be seen that the abnormal red region of wave velocity decreases significantly. At this time, the abnormal region of wave velocity on the working face 11224 is concentrated in the artificial working area and the front of mining, which are the corresponding abnormal regions caused by human disturbance. The results can be verified by the distribution of $V_p$, which proves the rationality of monitoring $A_n$.

### 3.1.3 Distribution of $V_G$ before and after coal seam tunneling

The distributions of $V_G$ before and after tunneling are shown in Fig. 8. It can be seen that the distribution of $V_G$ is slightly different compared with the distribution of $V_p$ and $A_n$. However, the overall anomaly region has roughly the same variation trend as the other two distributions. In Fig. 8(a), except for $V_G$ in the artificial operation area, which is close to 1, the values in other areas are all in a lower region (no more than 0.5), which can well reflect the stability of this region. Although it is in a valley position, its gradient is in a stable range and it is also considered a safer area. At the end of excavation, $V_G$ decreases significantly from 1.05 to 0.70. Many places in the alley are affected by the excavation operation, and the distribution of $V_G$ values is consistent with the abnormal areas in the above two sets of distributions maps, indicating that when the stress changes because of labor, $V_G$ changes more significantly, which is helpful to judge its outburst risk under the influence of stress changes.

In order to accurately obtain the stress distribution in different periods in this area, we can analyze the change rules of three indicators in 11224 working face area before and after coal roadway tunneling. In the gas extraction period before coal roadway excavation, the three indicators in the artificial operation area are all at high value points. Influenced by the geological structure, such as the valley, there is a sizeable abnormal area of high value between $V_p$ and $A_n$ of the 11224 working face. By comparing the distribution of $V_G$, we can judge that the high value area is not a risk area. In the

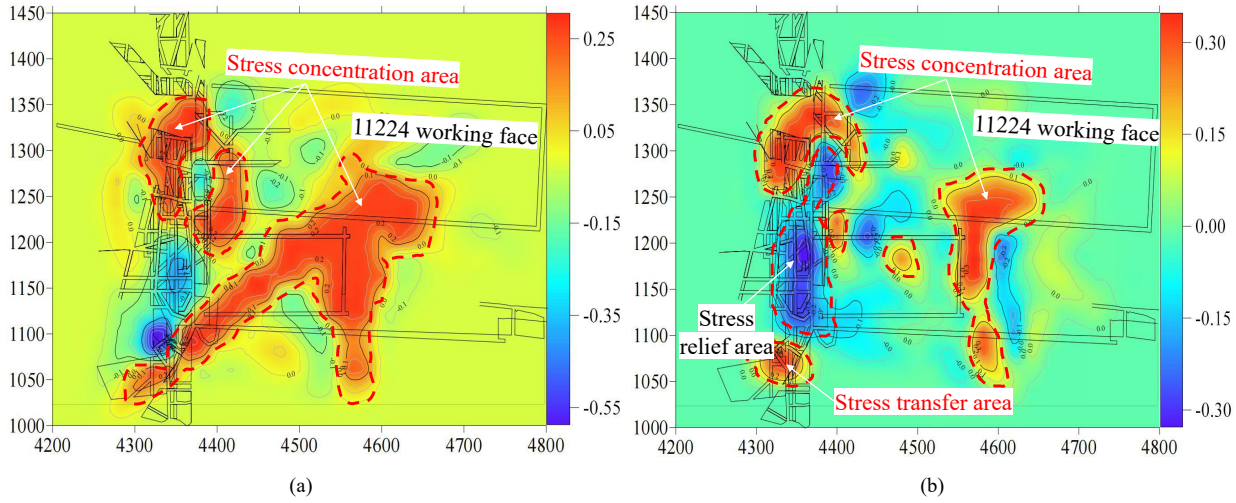


**Fig. 7**. Wave velocity anomaly coefficient $A_n$ distribution of coal seam before and after tunneling: (a) $A_n$ distribution before tunneling, (b) $A_n$ distribution after tunneling.

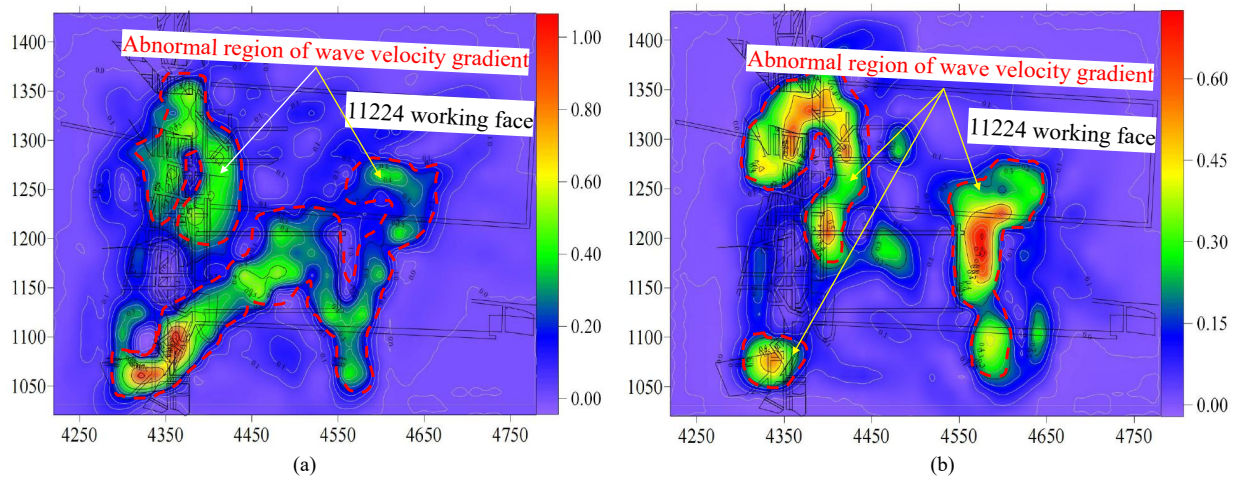


**Fig. 8**. Distribution of wave velocity gradient of coal seam before and after tunneling: (a) $V_G$ distribution before tunneling, (b) $V_G$ distribution after tunneling.

excavation period, due to the influence of the excavation work, there is an abnormal area of wave velocity in front of the head, which is a normal phenomenon. The distribution of the three indicators is basically the same, indicating that when the stress of the coal seam is disturbed, the change characteristics of $V_p$, $A_n$ and $V_G$ can confirm each other to achieve the purpose of safety monitoring.

## 3.2 Verification case 2: Coal seam hydraulic fracturing

Hydraulic fracturing is an important method for transforming the geological structure and reducing stress (Hui et al., 2022), widely used for coal seam outburst control. The section takes Longfeng coal mine as the engineering background. This is a production mine that adopts inclined shaft development. The designed production capacity is 0.9 Mt/a, and the area has 4 layers of recoverable coal seams. The mine is divided into three mining areas, and the construction location is the second mining area, that is, mining area II.

The coal seam wave velocity was tested by the SOS monitoring system, which is the same as that in Jinjia coal mine in Section 3.1 of this manuscript. The layout of seismic sensors is shown in Fig. 9. No. 1# and 2# sensors are arranged in the 59210 ventilating roadway, No. 3# and 4# sensors are arranged in the belt transportation main roadway, and No. 5# and 6# sensors are arranged in the 5922 ventilating roadway.

### 3.2.1 Distribution of $V_p$ before and after coal seam hydraulic fracturing

In order to evaluate the fracturing effect in the mining area, the seismic CT inversion of coal seam wave velocity field before and after complete fracturing was shown in Fig. 10.

It can be seen from the figure that there are two stress concentration areas before fracturing and the wave velocity is

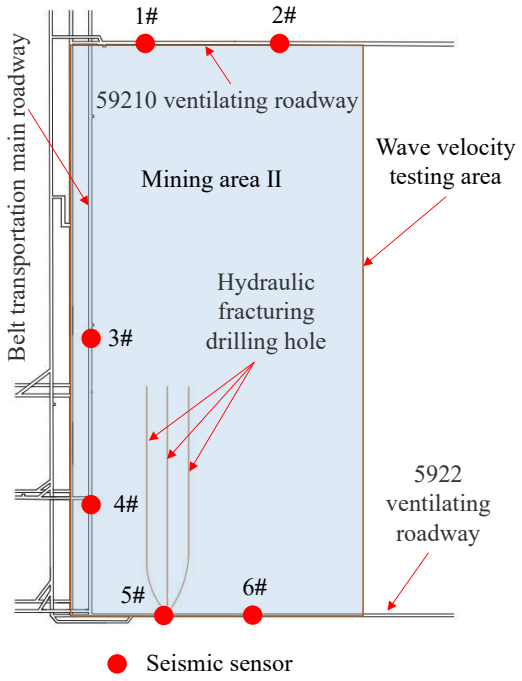


**Fig. 9**. Layout of seismic sensors in Longfeng coal mine.

mostly between 4.8 and 5.5 km/s. By comparison with the actual geological environment on site, it can be concluded that the stress concentration area is mainly affected by the buried depth, the surface structure and the uneven stress distribution of the coal rock itself, and there are more broken areas. After hydraulic fracturing, the two stress concentration areas disappear. The wave velocity is mostly between 4 and 5.1 km/s. The wave velocity in the whole area is significantly reduced, and the area with high wave velocity after fracturing is the artificial operation area. It can be concluded that after hydraulic fracturing, the wave velocity in the previously broken zone increases slightly. In contrast, the wave velocity in the stress concentration zone decreases significantly, and the regional stress field becomes more uniform. The wave velocity of the inversion results is between 3.7 and 6.0 km/s. If we only consider inside the Ming area II and remove the influence of the artificial operation area, the wave velocity is between 3.7 and 5.5 km/s. The maximum wave velocity is decreased, but the high wave velocity area is significantly reduced and the low wave velocity area is greatly increased. The hydraulic fracturing measures affect the east side of the drilling hole, significantly reducing the wave velocity and outburst risk in this area. The obtained results agree with the actual situation, proving the effectiveness of seismic wave CT inversion of stress field.

### 3.2.2 Distribution of $A_n$ before and after coal seam hydraulic fracturing

The $A_n$ inversion diagram of wave velocity anomaly coefficient before and after hydraulic fracturing in mining area II were shown in Fig. 11. According to the results, the distribution trend of $A_n$ after fracturing is also consistent with that of the distributions of $V_p$, indicating that the inversion results can confirm each other and the seismic wave CT inversion stress field has a high accuracy. Before fracturing, the wave velocity anomaly coefficient An takes a value between -0.2 and 0.16.

After fracturing, the positive abnormal area of wave velocity in mining area II has been greatly reduced, and the wave velocity anomaly coefficient $A_n$ is also significantly reduced. If we only consider the mining area II, the maximum wave velocity anomaly coefficient $A_n$ of coal seam decreases from 0.16 before fracturing to 0.08, which is already within the safe range. The artificial operation area is due to the positive abnormal wave velocity in hydraulic fracturing related construction. In summary, $A_n$ ranges from -0.2 to 0.32. If we only consider the interior of mining area II, the value of $A_n$ is between -0.2 and 0.12. Moreover, the abnormal state of stress in the area near the pressure fracture hole is greatly improved, and $A_n$ changes from 0∼0.16 before fracturing to -0.1∼0.08. Compared to that before fracturing, the range of positive abnormal wave velocity is greatly reduced and the maximum value is also decreased, which is consistent with the distribution of wave velocity.

### 3.2.3 Distribution of $V_G$ before and after coal seam hydraulic fracturing

The distribution of $V_G$ in mining area II before and after hydraulic fracturing is shown in Fig. 12. The distribution pattern of $V_G$ is slightly different compared to the $V_p$ and $A_n$. However, the overall anomaly region has roughly the same trend as the other two distributions. On the whole, the value of $V_G$ in mining area II is between 0 and 0.13. The abnormal region of $V_G$ variation corresponds to the stress concentration region in Figs. 10 and 11. The value of $V_G$ in these regions is high. It has a part greater than 0.1, the outburst risk region. After fracturing, the value of $V_G$ in mining area II is greatly reduced to below 0.1 in most areas. Except for a small part of the artificial operation area, $V_G$ in mining area II is slightly greater than 0.1, and the risk area of $V_G$ in mining area II has almost completely disappeared. The abnormal regions of $V_G$ are all at the edge of mining area II, and $V_G$ in this area is high due to manufactured construction and other factors.

By analyzing the wave velocity distribution of coal seam after the hydraulic outburst, the stress variation in the area around the borehole before and after hydraulic fracturing is obtained accurately. Before hydraulic fracturing, there are two stress concentration areas, most of which are between 4.8 and 5.5 km/s. After hydraulic fracturing, the two stress concentration areas disappear, most of which are between 4 and 5.1 km/s, and the wave velocity in the whole area decreases significantly. This trend of $V_p$ is consistent with $A_n$. However, according to the distribution of $V_G$, there is only one abnormal area at 59210 wind lane, corresponding to the stress concentration area in Figs. 10 and 11. After fracturing, the abnormal area of $V_G$ in mining area II is significantly reduced, the abnormal area of $V_p$, $A_n$ and $V_G$ are all at the edge of mining area II, and the artificial construction and other factors cause the anomaly coefficient $V_G$ of wave velocity change gradient to be high. It is proved that the hydraulic fracturing measures have a noticeable effect on the coal seam around the borehole, significantly reducing the wave velocity

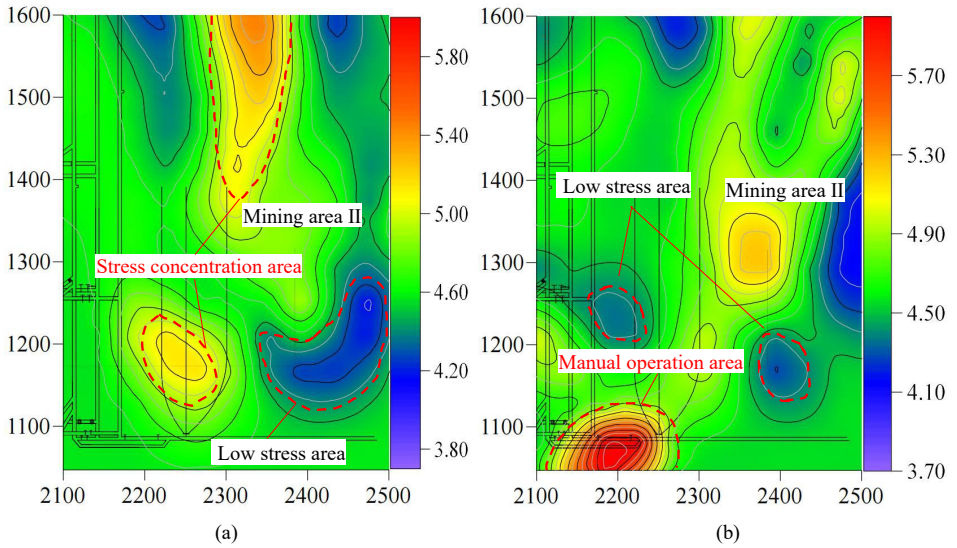


**Fig. 10**. Wave velocity distribution of coal seam before and after hydraulic fracturing: (a) $V_p$ distribution before hydraulic fracturing, (b) $V_p$ distribution after hydraulic fracturing.

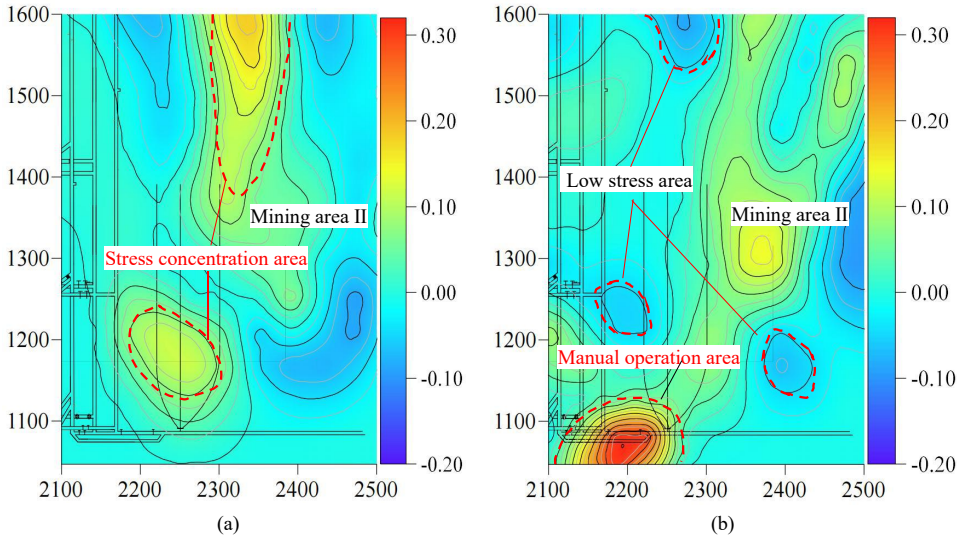


**Fig. 11**. Wave velocity distribution of coal seam before and after hydraulic fracturing: (a) $A_n$ distribution before hydraulic fracturing, (b) $A_n$ distribution after hydraulic fracturing.

and outburst risk in this area. The results agree with the actual situation, proving the effectiveness of the stress field inversion by seismic wave CT for outburst prediction.

## 4. Discussion

### *4.1 Correlation between seismic wave velocity and coal stress*

Some scholars have found that whether it is an uniaxial or triaxial experiment, the longitudinal wave velocity of coal and rock increases rapidly during the compaction stage. Li et al. (2019) carried out uniaxial loading experiments and uniaxial loading and unloading experiments of coal samples at different rates (Fig. 13). They found that the distribution of cracks, stresses and wave velocity in coal samples had a corresponding relationship. Then, they performed acoustic emission CT inversion calculations on mudstone samples and analyzed the wave velocity distribution characteristics at each loading stage (Fig. 14). In the elastic stage, the deformation of coal and rock samples had linear characteristics. Although the gaps between particles were further compacted, the gap density changed little compared with the initial stage due to the increase in pore pressure. The increase in wave velocity began to decrease. The specimen was damaged after entering the plastic zone, and the volume deformation increased. However, the damage mainly manifested by dislocation and slip between particles, so the wave velocity did not increase or decrease significantly at this stage. When many microscopic cracks were formed and connected to form cracks, the seismic wave velocity maintained the original value without much change.

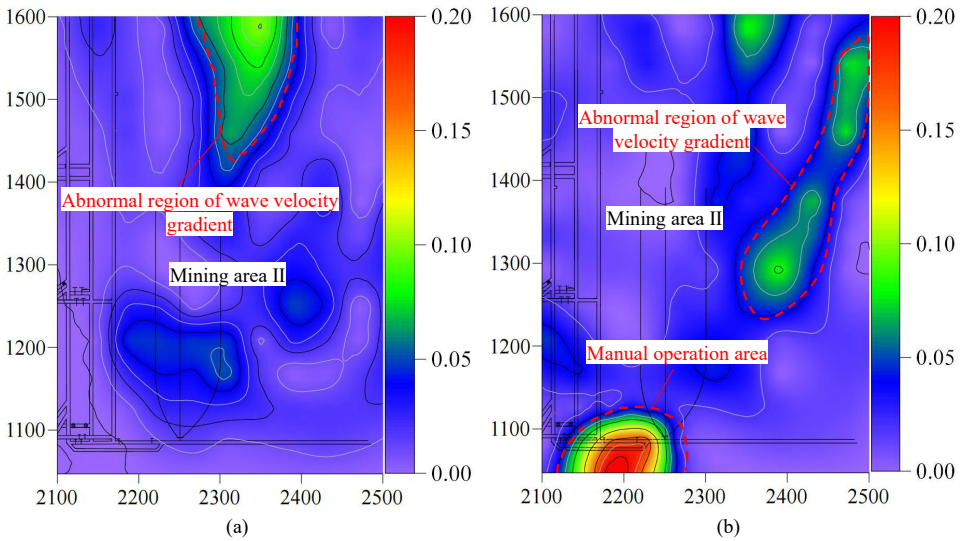


**Fig. 12**. Distribution of wave velocity gradient of coal seam before and after hydraulic fracturing: (a) $V_G$ distribution before hydraulic fracturing, (b) $V_G$ distribution after hydraulic fracturing.

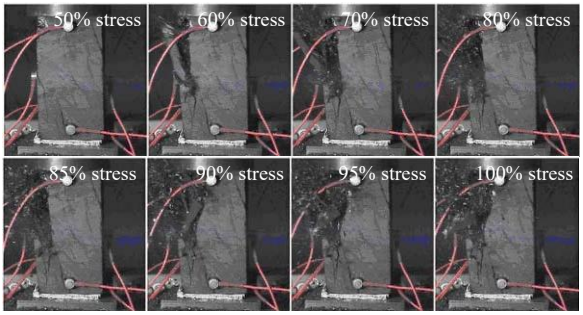


**Fig. 13**. Dynamic failure stage of coal sample.

Both stress and coal structure can affect wave velocity, which is consistent with the research results in this paper.

### 4.2 Technical applicability and prospects

The laboratory and on-site verification results indicate that $V_p$ can characterize the stress state of coal in the elastic-plastic stage, $A_n$ can judge the degree of coal breakage, and $V_G$ can identify the transition between high and low stress zones. In detecting the risk of coal seam outburst, a thorough comparative analysis should be conducted on these three indicators. Firstly, the position of high and low stress areas in the coal body should be preliminarily determined by the distribution of $V_p$. Secondly, the impact of fracture areas should be excluded by the distribution of $A_n$ to determine the areas with solid outburst risk. Thirdly, the distribution of $V_G$ should be used to identify areas with severe stress changes as a supplement to outburst risk areas. The comparison and analysis of these three indicators is beneficial for avoiding omissions and misjudgments of the outburst risk areas.

It is worth noting that the above three indicators are all derived from seismic wave detection and essentially belong to wave velocity indicators. They can only be used to identify the stress state of coal seam, which is closely related to wave velocity, and the detection effect of coal in the elastic-plastic stage is better than that in the plastic deformation or local instability state. Due to the multiple solutions of geophysical methods and the limitations of wave velocity indicators mentioned above, it is necessary to consider the actual geological structure of coal seam while detecting the coal and gas outburst risk. Drilling core analysis can compensate for this deficiency.

The seismic wave velocity detection method has been previously used in rock burst mine, while the research on coal and gas outburst risk detection is still in its initial stage. Due to the difference between rock burst and coal and gas outburst principle, further improvements to this method require a lot of experiments and field research. Besides, it needs to be combined with comprehensive analysis and research on the actual conditions of outburst mine.

## 5. Conclusions

The seismic wave velocity response law for the coal loading process and coal seam outburst risk were studied to identify areas with significant variation in stress disturbance in coal seams. The main results are as follows:

1) The wave velocity $V_p$, wave velocity anomaly coefficient $A_n$, and wave velocity gradient $V_G$ are all positively correlated with load, while the changes in $A_n$ and $V_G$ are more gentle than $V_p$. The degree of coal breakage can be judged by $A_n$, and the transition between high and low stress zones can be identified by $V_G$.
2) In areas affected by geological structures, such as valleys and mountain tops, coal seam $V_p$ and $A_n$ may exhibit anomalies. By analyzing the distribution of $V_G$, it can be determined that the area of high value has no outburst risk. During the excavation of the working face, the consistency of the three indicators is strong.
3) The stress relief zone boundary of hydraulic fracturing can be determined by the seismic wave velocity indicator. After hydraulic fracturing, the abnormal area of $V_G$ in mining area II is significantly reduced, and the abnormal

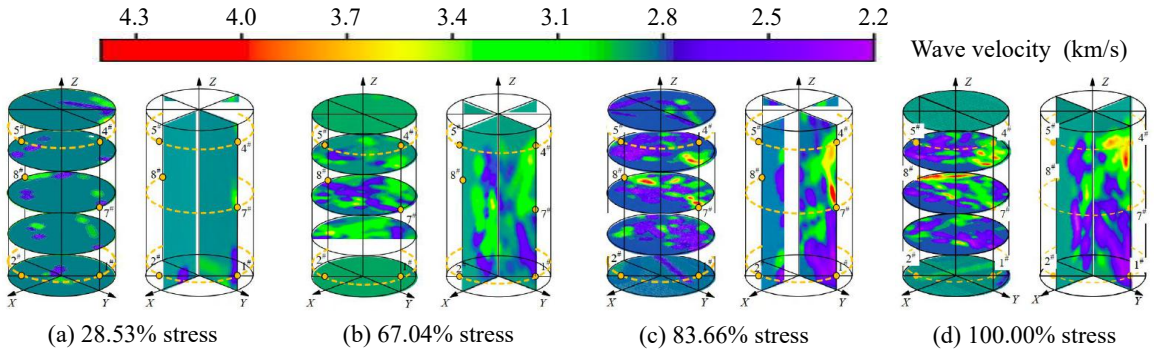


(a) 28.53% stress (b) 67.04% stress (c) 83.66% stress (d) 100.00% stress

**Fig. 14**. Wave velocity field evolution during mudstone sample failure.

area of $V_p$ and $A_n$ and $V_G$ is at the edge of mining area II.

4) To more accurately predict coal and gas outburst, the distribution of wave velocity indicators such as $V_p$, $A_n$, and $V_G$ can be analyzed during the seismic wave CT inversion detection process and combined with the actual geological structure characteristics of coal seams, such that areas with significant changes in stress disturbance on site can be identified.

## Acknowledgements

This work was supported by the National Natural Science Foundation of China (No. 52004016) and the Science and Technology Support Plan Project of Guizhou Province (No. [2023]515).

## Conflict of interest

The authors declare no competing interest.



## References

Aguado, M., Nicieza, C. Control and prevention of gas outbursts in coal mines, Riosa-Olloniego coalfield, Spain. International Journal of Coal Geology, 2007, 69(4): 253-266.

Alexander, S., Yuliya, D. Geophysical criterion of pre-outburst coal outsqueezing from the face space into the working. International Journal of Mining Science and Technology, 2019, 29: 499-506.

Bai, X., Jia, T., Zhang, Z., et al. Analysis of coal gas dynamic phenomenon in Xinmi coalfield. Coal Geology & Exploration, 2009, 37(4): 19-33. (in Chinese)

Black, J. Review of coal and gas outburst in Australian underground coal mines. International Journal of Mining Science and Technology, 2019, 29: 815-824.

Durucan, S., Cao, W., Cai, W., et al. Monitoring, assessment and mitigation of rock burst and gas outburst induced seismicity in longwall top coal caving mining. Paper ISRM-RDS-2019-002 Presented at ISRM Rock Dynamics Summit, Okinawa, Japan, 7-11 May, 2019.

Fatemeh, S., Guang, S., Hamid, R., et al. Numerical modelling of coal and gas outburst initiation using energy balance principles. Fuel, 2023, 334(1): 126687.

Frid, V., Vozoff, K. Electromagnetic radiation induced by mining rock failure. International Journal of Coal Geology, 2005, 64: 57-65.

Gong, S. Research and application of using mine tremor velocity tomography to forecast rock burst danger in coal mine. Beijing: China University of Mining and Technology, 2010. (in Chinese)

Hudecek, V. Analysis of safety precautions for coal and gas outburst-hazardous strata. Journal of Mining Science, 2008, 44(5): 464-472.

Hui, G., Chen, Z., Chen, S., et al. Hydraulic fracturing-induced seismicity characterization through coupled modeling of stress and fracture-fault systems. Advances in Geo-Energy Research, 2022, 6(3): 269-270.

Jun, T., Cheng, L., Yu, J., et al. Line prediction technology for forecasting coal and gas outbursts during coal roadway tunneling. Journal of Natural Gas Science and Engineering, 2016, 34: 412-418.

Katarzyna, K., Andrzej, N., Libor, S., et al. Rock and gas outbursts in copper mines: Use of brazilian tests to evaluate the work of disintegration of rock resulting from stresses produced by gas present in its porous structure. Rock Mechanics and Rock Engineering, 2022, 55(10): 6209-6225.

Khadijeh, A., Mehdi, N., Ramin, R. Prediction of coal and gas outburst risk by fuzzy rock engineering system. Environmental Earth Sciences, 2021, 80(15): 491.

Koziel, K., Janus, J. Force exerted by gas on material ejected during gas-geodynamic phenomena analysis and experimental verification of theory. Archives of Mining Sciences, 2022, 66: 491-508.

Lamaet, R., Bodziony, J. Management of outburst in underground coal mines. International Journal of Coal Geology, 1998, 35: 83-115.

Li, T., Cai, M., Cai, M. A review of mining-induced seismicity in China. International Journal of Rock Mechanics and Mining Sciences, 2007, 44(8), 1149-1171.

Li, Z., He, X., Dou, L., et al. Bursting failure behavior of coal and response of acoustic and electromagnetic emissions. Chinese Journal of Rock Mechanics and Engineering,

2019, 38(10): 2057-2068. (in Chinese)

Li, B., Wang, E., Li, Z., et al. Automatic recognition of effective and interference signals based on machine learning: A case study of acoustic emission and electromagnetic radiation. International Journal of Rock Mechanics and Mining Sciences, 2023, 170: 105505.

Liu, C., Chen, S., Zhao, J., et al. Geochemical characteristics and origin of crude oil and natural gas in the Southern Slope Zone, Kuqa Foreland Basin, NW China. Journal of Earth Science, 2022, 33(3): 820-830.

Liu, C., Li, S., Cheng, C., et al. Activation characteristics analysis on concealed fault in the excavating coal roadway based on microseismic monitoring technique. International Journal of Mining Science and Technology, 2017, 27(5): 883-887.

Lurka, A. Location of high seismic activity zones and seismic hazard assessment in Zabrze Bielszowice coal mine using passive tomography. International Journal of Mining Science and Technology, 2008, 18(2): 177-181.

Mlynarczuk, M., Skiba, M. An approach to detect local tectonic dislocations in coal seams based on roughness analysis. Archives of Mining Sciences, 2022, 67: 743-756.

Peng, Y., Qiu, L., Zhu, Y., et al. Multi-scale multivariate detection method for the effective impact range of hydraulic fracturing in coal seam. Journal of Applied Geophysics, 2023, 215: 105124.

Qiu, L., Liu, Z., Wang, E., et al., Early-warning of rock burst in coal mine by low-frequency electromagnetic radiation. Engineering Geology, 2020, 279: 105755.

Qiu, L., Song, D., Li, Z., et al. Research on AE and EMR response law of the driving face passing through the fault. Safety Science, 2019, 117: 184-193.

Rezaei, M., Davoodi, P., Najmoddin, I. Studying the correlation of rock properties with P-wave velocity index in dry and saturated conditions. Journal of Applied Geophysics, 2019, 169: 49-57.

Saito, S., Ishikawa, M., Arima, M., et al. Laboratory measurements of 'porosity-free' intrinsic $V_p$ and $V_s$ in an olivine gabbro of the Oman ophiolite: Implication for interpretation of the seismic structure of lower oceanic crust. Island Arc, 2015, 24: 131-144.

Salimbeni, S., Malusa, M., Zhao, L., et al. Active and fossil mantle flows in the western Alpine region unravelled by seismic anisotropy analysis and high-resolution P wave tomography. Tectonophysics, 2018, 731: 35-47.

Shi, S., Liu, Z., Feng, J., et al. Using 3D seismic exploration to detect ground fissure. Advances in Geo-Energy Research, 2020, 4(1): 13-19.

Shu, L., Liu, Z., Wang, K., et al. Characteristics and classification of microseismic signals in heading face of coal mine: Implication for coal and gas outburst warning. Rock Mechanics and Rock Engineering, 2022, 55(11): 6905-6919.

Sobczyk, J. A comparison of the influence of adsorbed gases on gas stresses leading to coal and gas outburst. Fuel, 2014, 115: 288-294.

Uyanik, O. Estimation of the porosity of clay soils using seismic P- and S-wave velocities. Journal of Applied Geophysics, 2019, 170: 103832.

Vlastimil, H., Milan, S. Forecast and prevention of coal and gas outbursts in the case of application of a new mining method-drilling of a coal pillar. Acta Montanistica Slovaca, 2010, 15(2): 102-108.

Wang, H., Cai, J., Su, Y., et al. Pore-scale study on shale Oil-$CO_2$-Water miscibility, competitive adsorption, and multiphase flow behaviors. Langmuir, 2023, 39: 12226-12234.

Xu, K., Fu, Q. Uneven stress and permeability variation of mining-disturbed coal seam for targeted CBM drainage: A case study in Baode coal mine, eastern Ordos Basin, China. Fuel, 2021, 289: 119911.

Xu, S., Xia, Y., Lu, M., et al. Fractal perspective on the effects of the acid-rock interaction on the shale pore structure. Energy and Fuels, 2023, 37: 6610-6618.

Xue, C., Shi, F., Gui F., et al. Accident case data-accident cause model hybrid-driven coal and gas outburst accident analysis: Evidence from 84 accidents in China during 2008-2018. Process Safety and Environmental Protection, 2022, 164: 67-90.

Yan, B., Zhu, C., Shen, C., et al. A novel ECBM extraction technology based on the integration of hydraulic slotting and hydraulic fracturing. Journal of Natural Gas Science and Engineering, 2015, 22, 571-579.

Yang, D., Chen, Y., Tang, J., et al. Comparative experimental study of methods to predict outburst risk when uncovering coal in crosscuts. Fuel, 2021, 288: 119851.

Ye, D., Liu, G., Ma, T., et al. The mechanics of frost heave with stratigraphic microstructure evolution. Engineering Geology, 2023, 319: 107119.

Zhang, G., Wang, E., Ou, J., et al. Regional prediction of coal and gas outburst under uncertain conditions based on the spatial distribution of risk index. Natural Resources Research, 2022, 31(6): 3319-3339.

Zhao, D., Xia, Y., Zhang, C., et al. A new method to investigate the size effect and anisotropy of mechanical properties of columnar jointed rock mass. Rock Mechanics and Rock Engineering, 2023, 56: 2829-2859.

Zheng, S., Long, Y., Zhong, G., et al. Numerical study on the mechanism of coal and gas outburst in the coal seam thickening area during mining. Energies, 2023, 16(7): 3288.

Zykov, S. V., Lee, U. H. About possibilities to improve current outburst hazard prediction based on updated mechanism of coal and gas outburst. Mining Report, 2016, 152(2): 161-170.